

**RAPID ANTIMICROBIAL SUSCEPTIBILITY TESTING
THROUGH IMPEDANCE SPECTROSCOPY USING LOW
CONDUCTIVITY ZWITTERIONIC BUFFERS**

PRAGYA SWAMI



**DEPARTMENT OF CHEMICAL ENGINEERING
INDIAN INSTITUTE OF TECHNOLOGY DELHI**

JULY 2022

© Indian Institute of Technology Delhi (IITD), New Delhi, 2022

**RAPID ANTIMICROBIAL SUSCEPTIBILITY TESTING
THROUGH IMPEDANCE SPECTROSCOPY USING LOW
CONDUCTIVITY ZWITTERIONIC BUFFERS**

by

PRAGYA SWAMI

Department of Chemical Engineering

Submitted

**in fulfilment of the requirements of the degree of Doctor of Philosophy
to the**



INDIAN INSTITUTE OF TECHNOLOGY DELHI

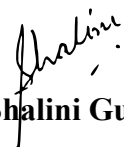
JULY 2022

CERTIFICATE

This is to certify that the thesis entitled “**Rapid antimicrobial susceptibility testing through impedance spectroscopy using low conductivity zwitterionic buffers**” being submitted by **Pragya Swami** for the award of the degree of **Doctor of Philosophy** in Chemical Engineering is a record of bonafied work carried out by her under my guidance and supervision at the Indian Institute of Technology Delhi.

The results contained in the thesis have not been submitted elsewhere, either in part or in full, to any other University or Institute for the award of any degree or diploma.

I certify that she has pursued the prescribed course of research.


Dr. Shalini Gupta

Associate Professor

Department of Chemical Engineering

Indian Institute of Technology Delhi

Hauz Khas, New Delhi -110016

India

ACKNOWLEDGEMENTS

I take this golden chance to express my heartfelt and deepest sense of gratitude to those who helped me to complete my dissertation. This thesis would not have been possible without the support, continuous concern and guidance of my advisor Dr. Shalini Gupta, Department of Chemical, IIT-Delhi. I am lucky to pursue Ph.D. under the supervision of her. I would like to express my warmest gratitude to her. Her positive thoughts and attitude, motivational talks, immense knowledge and teaching expertise improved my research capability, writing and presenting skills day by day. Her scientific approach and logical skills to solve the research problems increased my thought process, troubleshooting ability and confidence level. I am really thankful to her for encouraging and guiding me to move forward with more power and positive thinking in my Ph.D. life. She is the back-bone in developing my academic skills as well personality throughout the journey. I could not have imagine having a better advisor and mentor for my Ph.D. study. I feel proud to work under her supervision and wish her continued success in future endeavours.

Besides my advisor, I express my sincere gratitude to my research committee members - Profs. Gaurav Goel and A.N. Bhaskarwar from the Department of Chemical Engineering and Prof. Neetu Singh from Centre for Biomedical Engineering, IIT Delhi for the constant assessment of my work, guidance, insightful comments and suggestions that upgraded the quality of my Ph.D. work. I would also like to thank Prof. Vikas Manchanda from Maulana Azad Medical College, New Delhi and Dr. Venkataraman Sritharan from Global Hospital, Hyderabad for providing intelligent biological inputs and the clinical bacterial strains.

I would like to express my heartfelt thanks to all my colleagues. I am thankful to Satyam Anand, Ayush Sharma, Gajanand Verma and Anurag Holani for their scientific contribution as a

team in my Ph.D. projects. I would also grateful to Dr. Shruti Khanna for continuous guiding and improving my research communication throughout my Ph.D. Journey. She has always given me moral and metal support in my dark phase and guided me the right path as an elder sister. I would like to extend my sincere thanks to all my lab seniors Dr. Pramod Jagtap, Dr. Rohini Singh, Dr. Meenal Goel and Dr. Puja Prasad for sharing me their experiences and improving my research skills. I am also thankful to our lab manager Mr. Gaurav Jhakda who unconditionally supported me and did all possible assistance during my research work. I would also like to express my thanks to Vibhor Sharma, Neelam Choudhary, Rinky Bhatt whose friendship has always given me a support and unparalleled company, timely assistance and communications have been great sources of encouragement in my Ph.D career .

No words can express my gratitude and appreciation for my parents and family for everything they have done for me, especially my mother and grandmother who have been my pillar of strength throughout my PhD journey. I am deeply and thoroughly indebted to both for the freedom they have given to my choice of career.

Last but not the least, I would like to acknowledge IIT Delhi for giving me an opportunity to continue my research and the funding resources.

Pragya Swami

Abstract

Established antibiotic susceptibility testing (AST) techniques based on cell culture, gene amplification and mass spectroscopy are laborious, expensive and time consuming. They are inherently limited by the doubling rate of bacteria or bacterial DNA. Impedance spectroscopy, on the other hand, is a rapidly emerging tool for bacterial AST as it is simple, label-free, cost-effective, high-throughput and real-time. The current research in impedance biosensors mostly focuses on electrode design and cell enrichment strategies to enhance impedance signal, whereas the role of buffers in impedance spectroscopy is relatively unexplored. In my thesis, we have for the first time, investigated the use of Good's zwitterionic buffers (*e.g.*, HEPES) for impedance spectroscopy and illustrated their application for bacterial cell viability analysis and rapid AST. Our results show that zwitterionic electrolytes perform significantly better than standard electrolytes (*e.g.*, PBS) because of their large molecular size, lower concentrations at which they are used, high dissociation constants, and most importantly, higher ion-ion interactions (compared to PBS) which leads to the lowering of their conductivity and hence, increase in impedance signal. At the same time, zwitterionic buffers maintain cell vitality despite having low osmolality. With respect to cell viability in the presence of antibiotics, zwitterionic buffers play a crucial role as they allow measuring ionic changes due to bacterial death/growth with much greater sensitivity, reducing the overall detection time. We used two AST approaches in my thesis. In the first, ionic release due to antibiotic-triggered cell death was measured in HEPES buffer with or without a dielectrophoretic cell capture step depending on the electrode size. As a result, resistant and susceptible strains were readily distinguished within 30 min of cell-drug interaction. In the second approach, ionic release due to cell growth was measured in the presence of antibiotic in a low conductivity growth buffer that was pre-optimized with respect to HEPES buffer and Lb broth composition. The results were

obtained in 60 min (approximately 2 to 3 doubling cycles) which is 8 to 9 times faster than the conventional approaches. The various cell-drug combinations used included clinically susceptible and resistant strains of *Salmonella typhi*, *Staphylococcus aureus*, *Klebsiella pneumonia*, *Enterococcus faecalis* and *Escherichia coli* and nine different classes of antibiotics, selected based on their action mechanisms, cellular targets, and resistance patterns. Both systems were found to be highly specific and were further used for rapid MIC/MBC determination under 80 min paving way for efficient and rapid bacterial diagnosis and management.

सार

सेल कल्चर, जीन एम्प्लीफिकेशन और मास स्पेक्ट्रोस्कोपी पर आधारित स्थापित एंटीबायोटिक संवेदनशीलता परीक्षण (एसटी) तकनीक श्रमसाध्य, महंगी और समय लेने वाली हैं। वे स्वाभाविक रूप से बैक्टीरिया या जीवाणु डीएनए की दोहरीकरण दर से सीमित हैं। दूसरी ओर, प्रतिबाधा स्पेक्ट्रोस्कोपी, बैक्टीरियल एसटी के लिए एक तेजी से उभरता हुआ उपकरण है क्योंकि यह सरल, लेबल-मुक्त, लागत प्रभावी, उच्च-शुद्ध और वास्तविक समय है। प्रतिबाधा बायोसेंसर में वर्तमान शोध ज्यादातर प्रतिबाधा संकेत को बढ़ाने के लिए इलेक्ट्रोड डिजाइन और सेल संवर्धन रणनीतियों पर केंद्रित है, जबकि प्रतिबाधा स्पेक्ट्रोस्कोपी में बफर्स की भूमिका अपेक्षाकृत अस्पष्ट है। मेरी थीसिस में, हमने पहली बार प्रतिबाधा स्पेक्ट्रोस्कोपी के लिए गुड्स ज़िवटरियोनिक बफर्स (जैसे, हेपेस) के उपयोग की जांच की और बैक्टीरियल सेल व्यवहार्यता विश्लेषण और तेजी से एसटी के लिए उनके आवेदन को चित्रित किया। हमारे परिणाम बताते हैं कि ज़िवटरियोनिक इलेक्ट्रोलाइट्स अपने बड़े आणविक आकार, कम सांद्रता जिस पर उनका उपयोग किया जाता है, उच्च पृथक्करण स्थिरांक, और सबसे महत्वपूर्ण, उच्च आयन-आयन इंटरैक्शन (पीबीएस की तुलना में) के कारण मानक इलेक्ट्रोलाइट्स (जैसे, पीबीएस) की तुलना में काफी बेहतर प्रदर्शन करते हैं। जिससे उनकी चालकता कम हो जाती है और इसलिए, प्रतिबाधा संकेत में वृद्धि होती है। उसी समय, ज़िवटरियोनिक बफर्स कम ऑस्मोलैलिटी होने के बावजूद सेल जीवन शक्ति बनाए रखते हैं।

एंटीबायोटिक दवाओं की उपस्थिति में सेल व्यवहार्यता के संबंध में, ज़िवटरियोनिक बफर्स एक महत्वपूर्ण भूमिका निभाते हैं क्योंकि वे बैक्टीरिया की मृत्यु/वृद्धि के कारण अधिक संवेदनशीलता के साथ आयनिक परिवर्तनों को मापने की अनुमति देते हैं, जिससे समग्र पहचान समय कम हो जाता है। हमने अपनी थीसिस में दो एएसटी दृष्टिकोणों का इस्तेमाल किया। पहले में, एंटीबायोटिक-ट्रिगर कोशिका मृत्यु के कारण आयनिक रिलीज को इलेक्ट्रोड आकार के आधार पर एक डाइइलेक्ट्रोफोरेटिक सेल कैपचर चरण के साथ या बिना हेपेस बफर में मापा गया था। नतीजतन, सेल-ड्रग इंटरैक्शन के 30 मिनट के भीतर प्रतिरोधी और अतिसंवेदनशील उपभेदों को आसानी से पहचाना गया। दूसरे दृष्टिकोण में, सेल की वृद्धि के कारण आयनिक रिलीज को कम चालकता वृद्धि बफर में एंटीबायोटिक की उपस्थिति में मापा गया था जो हेपेस बफर और एलबी ब्रॉथ संयोजन के संबंध में पूर्व-अनुकूलित था। परिणाम 60 मिनट (लगभग 2 से 3 दोहरीकरण चक्र) में प्राप्त किए गए जो पारंपरिक तरीकों की तुलना में 8 से 9 गुना तेज है। प्रयोग किए गए विभिन्न सेल-दवा संयोजनों में साल्मोनेला टाइफी, स्टैफिलोकोकस ऑरियस, क्लेबसिएला निमोनिया, एंटरोकोकस फ़ेकलिस और एस्चेरिचिया कोलाई के नैदानिक रूप से अतिसंवेदनशील और प्रतिरोधी उपभेदों और उनके क्रिया तंत्र, सेलुलर लक्ष्यों और प्रतिरोध पैटर्न के आधार पर चयनित एंटीबायोटिक दवाओं के नौ अलग-अलग वर्ग शामिल थे। दोनों प्रणालियों को अत्यधिक विशिष्ट

पाया गया और कुशल और तेजी से जीवाणु निदान और प्रबंधन के लिए 80 मिनट के मार्ग के तहत तेजी से एमआईसी/एमबीसी निर्धारण के लिए उपयोग किया गया।

TABLE OF CONTENTS

CERTIFICATE	i
ACKNOWLEDGEMENTS	ii
ABSTRACT	iv
TABLE OF CONTENTS	ix
LIST OF FIGURES	xiv
LIST OF TABLES	xxv
DEFINITIONS OF TERM AND SYMBOLS USED IN THE TEXT	xxvii
ABBREVIATIONS	xxx
Chapter 1: INTRODUCTION	1
1.1 BACTERIAL INFECTION AND STATISTICS	2
1.2 ANTIMICROBIAL RESISTANCE AND ITS COMPLICATIONS	3
1.3 BACTERIAL DIAGNOSIS AND CHALLENGES.....	5
1.3.1 Detection and Identification	5
1.3.2 Susceptibility Testing	7
1.4 IMPEDANCE BIOSENSORS FOR BACTERIAL ANALYSIS.....	10
1.5 THESIS OBJECTIVES	11
1.6 THESIS LAYOUT.....	13
1.7 REFERENCES	14
Chapter 2: LITERATURE REVIEW	23
2.1 INTRODUCTION	24
2.2 THEORY	24
2.2.1 What is impedance spectroscopy	24
2.2.2 The real and imaginary parts of dielectric permittivity.....	26
2.2.2.1 Medium.....	26
2.2.2.2 Electrode polarization (EP).....	26
2.2.2.3 Bacteria	26
2.2.3 Frequency-dependence of impedance spectra and its relevance for bacterial suspension measurements	28
2.2.4 Modeling of impedance spectra	29

2.2.4.1 Maxwell's mixture theory	29
2.2.4.2 Equivalent circuit modeling.....	30
2.3 THEORY	32
2.3.1 Interfacial impedance	32
2.3.2 Medium resistance.....	34
2.3.3 Medium capacitance.....	36
2.4 CELL VIABILITY TESTING.....	37
2.5 LIMITATION OF PRESENT IMPEDANCE CELL VIABILITY STUDIES.....	42
2.6 ROLE OF BUFFERS.....	43
2.7 REFERENCES	45
Chapter 3: ROLE OF ZWITTERIONIC BUFFERS IN IMPEDANCE SPECTROSCOPY ..	54
3.1 INTRODUCTION	55
3.2 EXPERIMENTAL SECTION	57
3.2.1 Materials.....	57
3.2.2 Methods.....	58
3.2.2.1 Sample preparation.....	58
3.2.2.2 Impedance measurements.....	58
3.2.2.3 Cell culture	59
3.2.2.4 Dipole estimation.....	59
3.3 RESULTS AND DISCUSSION	60
3.3.1 Theoretical analysis of electrolytes in aqueous media.....	60
3.3.1.1 Ionic conductivity of electrolytes	61
3.3.1.1 Dielectric permittivity of electrolytes.....	63
3.3.2 Experimental analysis of electrolytes in aqueous media	65
3.3.2.1 Comparison of ideal versus experimental conductivity behaviour	65
3.3.2.1 Comparison of HEPES with other Good's buffers	69
3.3.2.3 Osmotic pressure on bacterial cells in low electrolyte solutions	70
3.3.2.4 Ionic measurements upon bacterial heat treatment	74
3.4 CONCLUSIONS	78
3.5 REFERENCES	78

Chapter 4: RAPID AST BY COMBINING DIELECTROPHORESIS WITH IMPEDANCE SPECTROSCOPY	83
4.1 INTRODUCTION	84
4.1.1 Correlation between impedance and DEP	85
4.2 EXPERIMENTAL SECTION	87
4.2.1 Materials	87
4.2.2 Methods	87
4.2.2.1 Buffer/bacterial suspension preparation	87
4.2.2.2 Antimicrobial activity assays	88
4.2.2.3 DEPIS Platform	88
4.2.2.4 Fluorescence cell imaging	89
4.3 RESULT AND DISCUSSION	89
4.3.1 Parameter selection and system optimization	89
4.3.2 Cell viability testing and dose-response curves	96
4.3.3 Microscopy analyses and the role of DEP	105
4.3.4 Rapid differentiation of resistant vs susceptible bacteria	108
4.4 CONCLUSION	110
4.5 REFERENCES	111
Chapter 5: RAPID AST USING IMPEDANCE SPECTROSCOPY	115
5.1 INTRODUCTION	116
5.2 EXPERIMENTAL SECTION	117
5.2.1 Materials	117
5.2.2 Methods	117
5.2.2.1 Antibiotic solution/bacterial suspension preparation	118
5.2.2.2 Antimicrobial activity assays	118
5.2.2.3 Equivalent circuit modeling	118
5.3 RESULTS AND DISCUSSION	119
5.3.1 Rapid antibiotic sensitivity analysis in HEPES buffer	119
5.3.2 Discussion	128
5.3.3 R/S strain differentiation through ECM	132
5.4 CONCLUSIONS	136

5.5 REFERENCES	136
Chapter 6: RAPID AST USING HEPES-MODIFIED GROWTH BUFFER AND IMPEDANCE SPECTROSCOPY	141
6.1 INTRODUCTION	142
6.2 EXPERIMENTAL SECTION	142
6.2.1 Materials	142
6.2.2 Methods	142
6.2.2.1 Buffer preparation	142
6.2.2.2 Antibiotic solution/Bacterial suspension preparation.....	143
6.2.2.3 Antimicrobial activity assays	143
6.2.2.4 Fluorescence cell imaging	143
6.3 RESULTS AND DISCUSSION	144
6.3.1 Measurement principle/concept	144
6.3.2 Parameter optimization	145
6.3.3 Rapid AST testing in growth buffer	150
6.4 CONCLUSIONS.....	153
6.5 REFERENCES	154
Chapter 7: SUMMARY AND FUTURE OUTLOOK	157
7.1 REFERENCES	160
APPENDIX A: MATHEMATICAL CALCULATIONS USED IN THE THESIS	161
A.1 Sample calculation for determining the signal to noise ratio.....	162
A.2 Bacterial double-shell model	162
A.3 pDEP bacteria capture calculation	164
A.4 Debye length calculatio.....	165
A.5 Cell constant calculation	165
A.6 Theoretical analysis of antibiotic-induced ionic release in cells.....	166
A.7 Experimental analysis of antibiotic-induced ionic release in cells	167
A.8 Calculation for conductivity change in medium due to addition of cells	167
A.9 Disc dissolution experiments for preparation of antibiotic solutions	168
A.10 Susceptibility testing through disc diffusion.....	171
A.11 Effect of antibiotic induced change in resistance and capacitance of system into overall impedance through ECM	171

A.12 Doubling time of bacteria calculation colony counting method	172
A.13 References	172
Curriculum Vitae	174

LIST OF FIGURES

- Figure 1.1** Top 10 leading causes of deaths worldwide. Image adapted from WHO Global Health Estimates 2019 & CDC 2021.....3
- Figure 1.2** Schematic showing different stages of antibiotic resistance transfer from resistant to healthy bacteria under the influence of improper antibiotic treatment. Image taken from ZME Science LLC research magazine, Romania.....4
- Figure 1.3** **The two stages of bacterial infection diagnosis: (a) pathogen identification and (b) susceptibility testing.** Representative examples of pathogen identification include chromogenic medium (*Escherichia coli* colonies shown in red and *Klebsiella pneumoniae* colonies shown in green-blue) [35], polymerase chain reaction (PCR) (targeted gene sequencing with fluorescence signal) [35], and mass spectrophotometry (MS) (peptide mass spectra) [47]. Representative examples of susceptibility testing include disc diffusion and broth dilution (gold standards) [48], live/dead cell imaging [48] and impedance sensing [49]. This image was created using Biorender s/w after adopting individual figures from Varadi *et al.*, 2017 [35], Diertvorst *et al.*, 2020 [48], Zhu *et al.*, 2016 [47] and Safavieh *et al.*, 2017 [49]).....7
- Figure 1.4** (a) Published trends of different biosensor techniques over the last 10 years searched using the keywords "name of the biosensor (*e.g.*, impedance)" and "bacterial detection" in Scopus. QCM and SPR stand for 'quartz crystal microbalance' and 'surface plasmon resonance', respectively. (b) Comparison of different AMR management techniques as a function of AST time.....10
- Figure 2.1** **Frequency-dependent permittivity and relaxation mechanisms for cell.** Ionic polarization is observed first, followed by interfacial and dipolar polarization. The figure is taken from a review article published in *Sensors* by Mehrotra *et. al.* in 2019 [12].....29
- Figure 2.2** The ECM for a cell positioned between two electrodes. Here, C_{dl} , C_{sol} , and C_{mem} represent the capacitance of the double layer, medium and cell membrane. While, R_{sol} , R_{mem} and

R_{cyto} symbolize the resistance of the medium, cell membrane and cytoplasm, respectively.....31

Figure 2.3 (a) Time-lapsed fluorescence micrographs at 400x magnification showing *E. coli*. (10^5 cfu/mL) attached to an electrode surface after 2 min (left) and 10 min (right) of incubation and **(b)** the corresponding increase in interfacial capacitance (denoted as C_{dl} in graph) as a function of cell concentrations (log Conc.) (adapted from Muñoz-Berbel *et al.*, 2007 [40], published in *Electrochem. commun.*).....33

Figure 2.4 (a) Schematic of cellular metabolism, metabolite production and ionic exchange across cell membranes by live bacteria into their surrounding environment (Figure is taken from Gómez *et al.*, 2002 [54], published in *Sens. Actuators B Chem.*) **(b)** Diagrammatic representation of impedance with bacterial growth. The figure is adapted from a review paper published in *Biotechnol. Adv.* by Yang and Bashir in 2008 [55].....35

Figure 2.5 Representative plots of solution capacitance (represented as C_{sol} in the graphs) as a function of time where (i), (ii) and (iii) indicate bacterial growth (increase in C_{sol}), bacterial death (decrease in C_{sol}) and bacterial stationary phase (C_{sol} constant) in suspension with time (Figure is adapted from Puttaswamy *et al.*, 2013, published in *Biosens. Bioelectron.* [67]).....36

Figure 2.6 Cell viability analysis by measuring DLC, bulk resistance, capacitance and cell size. (a) Impedance associated with various bacterial species (10^7 cfu/mL) at 10 Hz (DLC) after their selective binding to a pre-immobilized antimicrobial peptides (AMP) (Figure is adapted from Mannoor *et al.*, 2010 [78], published in *PNAS*). **(b)** Percentage normalized impedance at 1 kHz due to change in solution by *E.coli* (10^7 cfu/mL) spiked LB broth due to ampicillin interaction over 90 min (Image is taken from Safavieh *et al.*, 2017 [82], published in *ACS Appl. Mater. Interfaces*). **(c)** Change in the value of bulk capacitance of *E.coli* as a function of time after exposure to different bactericidal concentrations of ampicillin in culture medium (Figure is adapted from Puttaswamy, 2013 [67], published in *Biosens. Bioelectron.*). **(d)** Different resistant (Res) and susceptible (Sus) strains *E. coli* (EC), *S. aureus* (MSSA, MRSA) and *K. pneumonia* (KP) (5×10^7 cfu/mL) analysed

by impedance cytometry after 30 min exposure to different antibiotics at the S/R clinical breakpoints. Here, COL, GEN, CIP, COAMX, CFF, CFFOX stand for colistin, gentamicin, ciprofloxacin, co-amoxiclav, ceftazidime, ceftazidime, cefoxitin, respectively (Figure is taken from Spencer *et al.*, 2021 [86], published in *Nat. Commun.*).....41

Figure 3.1. Plot of Λ with Concentration^{0.5} for (a) HEPES, (b) PBS and (c) EPPS, PIPES and POPSO. The slope of the best-fit straight lines yielded the S value for HEPES to be nearly 6.5x more than that of PBS, indicating that ion-ion interactions were significantly stronger in HEPES. Similar results were obtained for EPPS, PIPES and POPSO with S_s values 4.4x, 9x and 6x that of PBS, respectively. The horizontal red lines in the top two graphs indicate the theoretically calculated values of ionic mobility (Λ^0) based on Kohlrausch’s law.....68

Figure 3.2 (a) Conductivity change ($\Delta\kappa$, where, $\kappa = \frac{c_c \cdot \cos \theta}{|\mu|}$ and θ is the measured impedance phase angle) of the medium due to time-dependent ionic release by *S. typhi* bacteria (10^7 cfu/mL) in three different low conductivity media. The results are plotted at 100 kHz using 50 μ m IDEs. **(b)** DC conductivity ($\Delta\kappa$) response of *S. aureus* (10^7 cfu/mL) in 15 mM HEPES and 0.0225x PBS buffers. $\Delta\kappa$ signal was indicative of the conductivity changes brought about by the bacteria in 45 min.....73

Figure 3.3 Viability of *S. aureus* in 15 mM HEPES and 0.0225x PBS buffers over 1 h.....74

Figure 3.4 The impedance experiments performed with heat-treated (b) *S. typhi* and (c) *S. aureus* bacteria in four different standard media (buffer pH was maintained at 7.4). The impedance results plotted after 60 min showed HEPES to have the best performance in terms of simultaneously high signal and high S/N values (given above respective signal bars; see model calculation in **Appendix A1**). Here, the standard deviation has been taken as measure of noise.....75

Figure 3.5 The frequency domain impedance spectra of live and heat-treated *S. aureus* cells (10^6 cfu/mL) obtained in (a) DI water, (b) 15 mM HEPES and (c) 1x PBS buffer using 100 μ m IDEs.....76

Figure 3.6 (a) Impedance change for *S. typhi* suspension (10^7 cfu/mL) in 15 mM HEPES buffer at 100 kHz using 50 μm IDEs. No significant change was observed over 1 h signifying the stability of live bacteria (did not release any ions) in the buffer in the absence of heat treatment. **(b)** Cell viability analysis of *S. typhi* in 15 mM HEPES buffer via plating method showed 100% cell death after 30 min of heat treatment (ii) compared to 1% cell death after 60 min in non-treated cells (i).....77

Figure 3.7 (a) The extent of heat-triggered ionic release in 15 mM HEPES buffer was found to be similar in *S. typhi* and *S. aureus*. The results were obtained using 50 μm IDEs. **(b)** Effect of electrode size. Results of heat-induced ionic release from *S. aureus* in 15 mM HEPES buffer showing higher measurable signal response in 100 μm IDEs compared to 50 μm77

Figure 4.1 Schematic of the impedance spectroscopy combined with DEP biosensor illustrating the chronological sequence of events involved in the detection process. The insets depict actual fluorescence micrographs of the bottom electrodes captured at various time points. Here, the live bacteria are green and the dead ones as red.....90

Figure 4.2 (a) i, ii and iii represent a double shell, single shell, and equivalent bacterial dielectric model. Here, σ , ϵ and $\tilde{\epsilon}$ stand for conductivity, relative permittivity and effective permittivity of the bacteria, respectively. Similarly, a , a_{mem} and a_{wall} represent the radius of the cytoplasm, thickness of the cell membrane and thickness of the cell wall, respectively. **(b)** The real part of CM factor for live bacterium plotted as a function of frequency for different medium conductivities σ_{sol} in the 0.001 to 0.4 S/m range.....91

Figure 4.3 (a) Differential impedance values ($|\Delta I|$) at 100 kHz frequency for several NaCl concentrations in low conductivity media: DI water (0.0001 S/m), 0.1 mM PBS (0.02 S/m), 15 mM HEPES (0.04 S/m), 30 mM HEPES (0.075 S/m), 40 mM HEPES (0.1 S/m), 0.5 mM PBS (0.1 S/m) and 1 mM PBS (0.18 S/m). **(b)** The $|\Delta I|$ response at 100 kHz measured as a function of time for *S. typhi* bacteria (10^7 cfu/mL) suspended in different media. The signal was indicative of the number of ions released by the bacteria. **(c)** Time-resolved pDEP capture (20 V_{pp} , 5 MHz) of *S. typhi*

bacteria (10^7 cfu/mL) at the electrode surface. Here, one field of view (FOV) represents $37,000 \mu\text{m}^2$ surface area. **(d)** Measured impedance and phase angle spectra of 15 mM HEPES buffer in the 1 kHz to 10 MHz frequency range. Lines *F1* and *F2* indicate analytically-derived dominating impedance factors in this frequency domain.....93

Figure 4.4 Differential impedance change as a function of NaCl concentration in 15 mM HEPES buffer at 100 kHz. The sensitivity and the lower limit of detection (LOD) were found to be 252 ohm/mM and 0.1 mM, respectively. The formula used for LOD determination was $C_{\text{LOD}} = 3\sigma/S_{\text{impedance}}$, where σ is the standard deviation (SD) ($n = 3$) and $S_{\text{impedance}}$ is the slope (or sensitivity) obtained after linear fitting of the experimental data with 3SD ($R^2 = 0.97$).....94

Figure 4.5 The impedance of bacterial suspensions (10^7 cfu/mL) in 15 mM HEPES buffer before ($t = 0$) and after ($t = 30$ min, 60 min) the application of DEP to see the impedance variation over a large frequency domain (1 kHz to 10 MHz).....95

Figure 4.6 One-hour dose response curves obtained using DEPIS platform for *S. typhi* bacteria (10^7 cfu/mL) in the presence of **(a)** PMB (0.00625 - 20 μM or 8 ng/mL - 26 $\mu\text{g/mL}$) and **(b)** levo (0.05 - 25 μM or 18 ng/mL - 9 $\mu\text{g/mL}$) antibiotic. The values inside the bars indicate % cell death determined using the plating method. Also, ‘ns’ stands for not significant ($p > 0.05$) and *, **, *** imply $0.01 \leq p \leq 0.05$, $0.001 \leq p < 0.01$ and $p < 0.001$, respectively. **(c)** Impedance changes obtained for different cell-drug combinations at 5 μM drug concentration (also see Table 1). **(d)** Proposed phenomena for bacterial capture through DEP and ion concentration measurement as a function of antibiotic concentration in our chip through IS. Here, the ΔI response is small in *region I* (low ionic release at the electrodes with high cell capture) and *region III* (high ionic release in bulk at low cell capture), whereas ΔI response is high in *region II* (moderate ionic release at the electrodes with moderate cell capture) and *region IV* (excessive ionic release in bulk without cell capture).....98

Figure 4.7. Cell viability analysis of *S. typhi* using the standard plating method. **(a) & (b)** show the representative MBC plots against PMB (0.00625 - 20 μM or 8 ng/mL - 26 $\mu\text{g/mL}$) (a) and levo (0.05 - 25 μM or 18 ng/mL - 9 $\mu\text{g/mL}$) (b) drugs after 1 h of drug exposure and overnight growth.

(c) Cell viabilities obtained after 1 h of fixed concentration (5 μM) drug exposure with different antibiotics.....99

Figure 4.8 The frequency sweeps of impedance spectra as a function of (a, b) drug concentration at $t = 60$ min and (c, d) time at MBC_{50} . These data are collected for *S. typhi* (10^7 cfu/mL) in the presence of PMB (0.00625 - 20 μM or 8 ng/mL - 26 $\mu\text{g/mL}$) (a, c) and levo (0.05 - 25 μM or 18 ng/mL - 9 $\mu\text{g/mL}$) (b, d).....100

Figure 4.9 MBC plot obtained for *S. typhi* and levo (18 ng/mL - 9 $\mu\text{g/mL}$) at the end of 30 min from the start of the cell-drug incubation period. The results showed similar trends to Figure 4.6b suggesting that our technique can perform cell viability analysis in just 30 min.....101

Fig. 4.10 Cell viability analysis using UV-visible spectroscopy. The graph shows time-dependent absorbance values (O.D._{600}) of *S. typhi*. (10^7 cfu/mL) in the presence of different antibiotics (5 μM final concentration). All the results were below the reliability limit of the instrument (~ 0.1 O.D.) and did not show proper correlation with the culture data.....102

Figure 4.11 Change in the impedance of bacterial suspension (10^7 cfu /mL) in 15 mM HEPES buffer in the lower frequency range (< 10 kHz) with and without DEP.....105

Figure 4.12 Microscopy analyses and role of DEP. (a) Fluorescence images depicting live and dead *S. typhi* collected on the bottom electrode surface with or without DEP and in the presence of different PMB drug concentrations (No drug, $\text{MBC}_{50} = 0.025$ μM (32 ng/mL) and $\text{MBC}_{100} = 5$ μM) (6.5 $\mu\text{g/mL}$). The live bacteria appear green under the FITC filter and the dead bacteria appear red using the Tx-Red filter. The top two panels are complementary to each other as are the bottom two panels except the first two images of the first column (with DEP no drug case). In the FITC panels, the black regions represent the electrodes and green regions indicate glass, whereas, in the Tx-Red rows, red stands for the electrode and black is glass. (b) Quantitative analyses of (a) after averaging over six such images. Here, FOV per image is equal to 37000 μm^2 . (c) Comparative impedance data obtained with and without DEP at various PMB concentrations highlighting the essential role of

DEP in making the process more sensitive. All data are reported at 100 kHz after 30 min of drug exposure.....107

Figure 4.13. Complementary fluorescence micrographs of (a) live (green) and (b) dead (red) *S. typhi* taken at $t = 30$ min on the bottom surface in the presence of DEP and $20 \mu\text{M}$ ($26\mu\text{g/mL}$) PMB. Most of the bacteria were either lysed in the bulk or found dead at the bottom surface. No live bacteria were found on the bottom surface.....108

Figure 4.14. (a) Impedance data for EFS and EFR after one hour of drug exposure ($0.5 \mu\text{M}$ ($0.18 \mu\text{g/mL}$) levo). Here, the lack of signal change highlights that our method cannot differentiate resistance developed against drugs that act inside the cytoplasm. **(b)** Impedance data for MSSA and MRSA after one hour of drug exposure ($0.2 \mu\text{M}$ ($0.08 \mu\text{g/mL}$) methicillin). The significant difference in signal indicates the efficacy of our approach in differentiating resistance developed against drugs that act on the cell wall. The results are plotted at 100 kHz and the values reported inside each bar graph indicate the % bacterial cell death at that condition as determined by the plating method. ‘ns’ stands for not significant ($p > 0.05$) and ‘*’ implies $0.01 \leq p \leq 0.05$110

Figure 5.1 Schematic showing the extension of electric field lines up to a greater height into the bulk medium in case of larger size IDEs.....117

Figure 5.2 Impedance sensor for rapid AST measurements via ionic changes due to cell death using large sized electrode ($100 \mu\text{m}$) and low conductivity buffer (15 mM HEPES).....119

Figure 5.3 (a) Representative culture plates showing the cell viability of *S. aureus* (10^7 cfu/mL) after 30 min of VA exposure at different concentrations. **(b)** Linear differential impedance measured as a function of % cell death in *S. aureus* exposed to different concentrations of VA for 30 min **(c)** Sigmoidal plot of differential impedance change after 30 min of exposure of *S. aureus* to different VA concentrations (corresponding cell death is mentioned on top of the scatter symbols). The dotted line indicates the fitted sigmoidal curve with an R^2 of 0.99.....120

Figure 5.4 MSSA and MRSA screening against methicillin. Time-dependent ΔI response obtained for MET (7.5 $\mu\text{g}/\text{mL}$) against different strains of MRSA (green) and MSSA (red), and for VA (7.5 $\mu\text{g}/\text{mL}$) against one strain each of MRSA and MSSA (blue). The average % cell death values determined by culture methods are mentioned in the respective bars. ‘ns’ stands for not significant ($p > 0.05$) and *, **, *** represent $0.01 \leq p \leq 0.05$, $0.001 \leq p < 0.01$ and $p < 0.001$, respectively. The cell concentration used was 10^7 cfu/mL in all the experiments.....121

Figure 5.5 Frequency dependent impedance spectra obtained for (a) MSSA and (b) MRSA (10^7 cfu/mL) in the presence of 7.5 $\mu\text{g}/\text{mL}$ of MET.....122

Figure 5.6 Plating data showing the number of colonies formed with (i & iii) MRSA and (ii & iv) MSSA after overnight incubation on agar gels. The colony count is mentioned in the inset. Here, data in (i, ii) is in the absence of drug and (iii, iv) is after 30 min of 7.5 $\mu\text{g}/\text{mL}$ MET exposure (iii, iv).....123

Figure 5.7 (a) The differential impedance response measured for MSSA and MRSA in the presence of 7.5 $\mu\text{g}/\text{mL}$ of MET. Comparison of the S/N (mentioned above the respective impedance signal bars; see Appendix A.1) in 50 and 100 μm IDEs showed a higher S/N in 100 μm IDEs in both cases in spite of its weaker electric field strength [3]. **(b)** Frequency spectra of impedance and phase angles in 15 mM HEPES buffer using 100 μm IDEs.....123

Figure 5.8 Minimum detectable cell concentration using 100 μm IDEs. The data are depicted for MSSA in the presence of 7.5 $\mu\text{g}/\text{mL}$ of MET.....124

Figure 5.9 Time-dependent screening of resistant and susceptible strains. ΔI response for four surface-acting antibiotics (colistin methanesulfonate (CMS), imipenem (IMP), ceftazidime (CF), ampicillin (AMP)) and four cytoplasm-active drugs (rifampicin (RIF), trimethoprim (TR), gentamicin (GEN), ciprofloxacin (CIP)) against the R/S strains of *S. aureus* (SA), *E. coli* (EC) and *K. pneumoniae* (KP) after 30 min of drug exposure. The results based on statistical significance variation in ΔI indicate that our cell death-based ionic change approach works only for surface-acting drugs. The average % cell death values determined by culture methods are mentioned in the

respective bars. ‘ns’ stands for not significant ($p > 0.05$) and *, **, *** represent $0.01 \leq p \leq 0.05$, $0.001 \leq p < 0.01$ and $p < 0.001$, respectively.....127

Figure 5.10 Schematic representation of our system for the purpose of equivalent circuit modelling.....132

Figure 5.11 Time-resolved change in (a) medium resistance, (b) cell membrane/wall capacitance and (c) EDL due to MET interaction with MSSA/MRSA. The % change in the value of each parameter by ECM.....133

Figure 5.12 Time-resolved change in impedance at 100 kHz for MSSA and MRSA in the presence of MET due to change in (a) R_{sol} , (b) $C_{mem-wall}$, and (c) C_{dl} . The change in impedance was primarily due to the change in R_{sol} whereas, that due to other parameters was negligible (< 0.1 ohms) (see calculation in Appendix A.11).....133

Figure 5.13 Proportion of time-dependent change in impedance at 100 kHz due to change in R_{sol} , $C_{mem-wall}$, and C_{dl} for MSSA and MRSA in presence of MET.....134

Figure 5.14 (a) The change in solution resistance (ΔR_{sol}) obtained by fitting and (b) the change in total impedance (ΔI) obtained by experiments due to the interaction between MSSA or MRSA bacteria and MET showed good agreement with each other. The results are reported as a function of time at 100 kHz frequency.....134

Figure 5.15 Change in (a) medium resistance, (b) cell membrane/wall capacitance and (c) EDL with time for gentamicin-susceptible and gentamicin-resistant *S. aureus* strains in the presence of gentamicin.....135

Figure 6.1 Concept of impedance sensor for rapid AST measurements via metabolite changes due to cell growth in a modified LCGB.....145

Figure 6.2 (a) Time-dependent growth study for *E. coli* performed using UV-visible spectroscopy in LB broth and different LCGB compositions (LCB and varying amounts of LB broth) at earlier time points. **(b)** Growth buffer optimization study. The medium conductivity obtained for different buffer compositions was plotted on the X-axis against the normalized values of differential impedance (left Y-axis) and bacterial growth (right Y-axis) obtained for *E. coli* after 60 min. The Y-axes data were normalized with respect to the highest and lowest values measured.....146

Figure 6.3 (a) *E. coli* (initial concentration 10^8 cfu/mL) growth study performed using UV-visible spectroscopy in LB broth and optimized LCGB over 24 h. **(b)** Normalized absorbance plot for *E. coli* in both buffers in the first 2.5 h. The 3x lower slope in LCGB indicated a bacterial doubling time of 60 min compared to 20 min in LB broth.....147

Figure 6.4 *E. coli* cell growth assessment through plate colony counting (a) and optical microscopy (b) methods. (a) The average doubling time was found 55 min through the colony counting method (see Appendix A.12). (b) The results shown here are representative of a larger set of cells, some of which divided in less than 60 min, while others took a longer time. The average was obtained around 60 min.....147

Figure 6.5 Linear ΔI response for *E. coli* as a function of its doubling cycles (n), where one doubling time was 60 min (as obtained from (b)) and the initial cell concentration (n = 0) was 10^7 cfu/mL.....148

Figure 6.6 (a) Time-resolved frequency spectra of impedance (break Y-axis) and **(b)** the corresponding phase angles at 0 min for *E. coli* (10^7 cfu/mL) growth in LCGB. The maximum shift was observed at 100 kHz with a phase angle of -4°149

Figure 6.7 Time-dependent impedance measurements performed with *E. coli* in LCGB. **(a)** Effect of electrode size. Experiments performed with 50 and 100 μm IDEs using 10^7 cfu/mL cells showed consistently higher S/N in 100 μm IDEs (representative S/N values mentioned above the impedance

signal bars at 80 min). **(b)** The lowest limit of detection in 100 μm IDEs was found to be 10^6 cfu/mL.....149

Figure 6.8 Time-dependent growth curves for **(a)** *S. aureus* and **(b)** *K. pneumoniae* in LCGB and LB broth. By comparing the slopes of the two buffers, the doubling time of *S. aureus* and *K. pneumoniae* was estimated as 56 min and 50 min, respectively, in LCGB.....150

Figure 6.9 Impedance change due to *E. coli* growth in LCGB with and without the presence of levofloxacin taken at different concentrations, plotted as a function of **(a)** time and **(b)** drug concentration. The conductivity-matched no growth 0.09x PBS buffer (0.14 S/m) was used as positive control.....151

Figure 6.10 MIC curve for *E. coli* (10^7 cfu/mL) against levofloxacin obtained in 80 min. The MIC value was found to be 90 ng/mL. **(e)** Plating data corresponding to the MIC plot in (d) with (i) no drug at time $t = 0$, (ii) 90 ng/mL drug at $t = 0$, (iii) no drug at $t = 80$ min and (iv) 90 ng/mL drug at $t = 80$ min.....151

Figure 6.11 Rapid antibiotic sensitivity analysis in clinical isolates using novel growth buffer. The impedance response of two surface-acting drugs (cefoxitin (CF) and methicillin (MET)) and one cytoplasm-active antibiotic (ciprofloxacin (CIP)) against R/S strains of *S. aureus* (SA) and *E. coli* (EC) after 60 min of drug exposure in LCGB. 2 $\mu\text{g/mL}$ of cefoxitin, 0.0625 $\mu\text{g/mL}$ of ciprofloxacin, and 0.5 $\mu\text{g/mL}$ of methicillin used for the resistivity analysis. The results based on statistical significance variation in ΔI indicated that our cell growth-based metabolic change measurement works irrespective of the drug type. ‘ns’ stands for not significant ($p > 0.05$) and *, **, *** represent $0.01 \leq p \leq 0.05$, $0.001 \leq p < 0.01$ and $p < 0.001$, respectively.....152

Figure 6.12 Time-lapse differential impedance measurements for R/S strains of *S. aureus* (SA) and *E. coli* (EC) in LCGB in the presence of **(a)** 2 $\mu\text{g/mL}$ of cefoxitin, **(b)** 0.0625 $\mu\text{g/mL}$ of ciprofloxacin, and **(c)** 0.5 $\mu\text{g/mL}$ of methicillin. (The concentration of antibiotic are estimated through disk diffusion (Appendix 9).).....153

LIST OF TABLES

Table 1.1 Bacterial detection and AST techniques.....	9
Table 2.1 A comparison of the three modes of impedance detection of bacterial suspensions.....	37
Table 2.2. A list of media used for different applications of bacterial sensing via impedance spectroscopy.....	43
Table 3.1. Comparison between ideal and experimentally measured conductivities of PBS buffer at various dilutions.....	66
Table 3.2. Comparison between ideal and experimentally measured conductivities of HEPES buffer at various dilutions. The actual electrolyte concentration is 50% of buffer concentration at pH 7.4. Large deviations from ideality were seen even at low electrolyte concentrations.....	66
Table 3.3. Conductivity measurements of different zwitterionic buffers at 40 mM and pH = pKa ₂ + 1 (where all the buffers exist as only anions). The conductivity of PIPES and POPSO was found to be approximately twice as that of HEPES and EPPS due to the presence of two negatively charged sulfide ions per molecule instead of one. The molecular structures were geometrically optimized in Avogadro (s/w version 1.2.0) [51] to calculate their ionic sizes.....	70
Table 3.4 Theoretical estimate of suction pressure generated on bacterial cells when placed in three different media at various concentrations.....	72
Table 4.1 The diffusion time of ions released from the bacterial cells was estimated using Einstein's equation ($x^2 = 2D_s t$), where D , t and x represent self-diffusivity, time, and distance, respectively.....	91
Table 4.2. List of bacterial strains and antibiotics used in our cell-drug interaction studies.....	97

Table 4.3 Comparison of the BC ₁₀₀ and BC _{lysis} values of PMB and levo obtained for susceptible <i>S. typhi</i> using our method with the MIC values obtained using the standard agar dilution method as reported in the literature [32,33].....	99
Table 4.4. Conductivities of different antibiotics in 15 mM HEPES buffer.....	101
Table 5.1 Confusion matrix for determining the sensitivity and specificity of our impedance method with respect to the gold standard disk diffusion method.....	124
Table 5.2 Performance comparison of our impedance method with other existing methods for MRSA screening.....	125
Table 5.3 Antibiotics used in our study along with their class, mode of action and possible resistance mechanisms. All the drugs except trimethoprim and ciprofloxacin were bactericidal in nature. ‘*’ indicates bacteriostatic drug.....	126
Table 5.4 Conductivities of different antibiotics in 15 mM HEPES buffer.....	128
Table 6.1 Cell-antibiotics combination used in our study along with their antibiotic activity, and possible resistance mechanisms.....	145

DEFINITIONS OF TERMS AND SYMBOLS USED IN THE TEXT

Symbol	Notes	Units
I	Absolute impedance	Ohm (Ω)
\tilde{I}	Complex impedance	Ω
I'	Real part of impedance	Ω
I''	Imaginary part of impedance	Ω
\tilde{K}	Complex conductivity	Siemens meter ⁻¹ (S/m)
K' or κ	Real part of conductivity/DC conductivity	S/m
K''	Imaginary part of conductivity	S/m
C_c	Geometrical cell constant	meter ⁻¹ (m ⁻¹)
ω	Angular frequency	Hertz (Hz)
$\check{\epsilon}$	Complex permittivity	Farad meter ⁻¹ (F.m ⁻¹)
ϵ'	Real part of permittivity	F.m ⁻¹
ϵ''	Imaginary part of permittivity	F.m ⁻¹
θ	Phase angle	Degree (°)
C_{dl}	Double layer capacitance	F.m ⁻²
R_{sol}	Solution resistance	Ω
C_{sol}	Solution capacitance/Bulk capacitance	F.m ⁻²
f_{cm}	The Clausius–Mossotti factor	Unit less
$Re(f_{cm})$	Real part of the Clausius–Mossotti factor	Unit less
$\phi/v_1/v_2$	Volume fraction	Unit less
$\check{\epsilon}_{cell}$	Complex permittivity of cell	F.m ⁻¹
$\check{\epsilon}_{sol}$	Complex permittivity solution	F.m ⁻¹
$\check{\epsilon}_{mix}$	Complex permittivity cell and solution	F.m ⁻¹
$\check{\epsilon}_{cyto}$	Complex permittivity cell cytoplasm	F.m ⁻¹
$\check{\epsilon}_{mem}$	Complex permittivity cell membrane	F.m ⁻¹
$\check{\epsilon}_{wall}$	Complex permittivity cell wall	F.m ⁻¹
$\check{\epsilon}_{cyto-mem}$	Complex permittivity cell cytoplasm and membrane	F.m ⁻¹
$\check{\epsilon}_{cyto-mem-wall}$	Complex permittivity cell cytoplasm, membrane and wall	F.m ⁻¹
$\check{\epsilon}_{eff}$	Complex permittivity of inner sphere of the two phase dielectric spheres	F.m ⁻¹
$\check{\epsilon}_1$	Complex permittivity of outer layer of the two phase dielectric spheres	F.m ⁻¹
$\check{\epsilon}_2$	Complex permittivity of the two phase dielectric spheres	F.m ⁻¹
v_1 and v_2	Volume Fraction	Unit less
C_{mem}	Capacitance of cell membrane	F.m ⁻²
C_{wall}	Capacitance of cell wall	F.m ⁻²

$C_{mem-wall}$	Capacitance of cell membrane and cell wall	$F.m^{-2}$
R_{mem}	Resistance of cell membrane	Ohm meter ² ($\Omega.m^2$)
R_{wall}	Resistance of cell wall	$\Omega.m^2$
R_{cyto}	Resistance of cell cytoplasm	$\Omega.m^2$
A	Electrode surface area	Meter ²
ϵ_{dl}	Permittivity of double layer	$F.m^{-1}$
D	Distance between two electrodes	Meter
κ_+	DC conductivity of cations	S/m
κ_-	DC conductivity of anions	S/m
λ_+	Molar conductivity of the cation	Siemens meter ² mole ⁻¹ ($S.m^2.mol^{-1}$)
λ_-	Molar conductivity of the anion	$S.m^2.mol^{-1}$
C_+	Cation molar concentration	Mole.meter ⁻³ ($mol.m^{-3}$)
C_-	Anion molar concentration	$mol.m^{-3}$
C_{el}	Electrolyte concentration	$mol.m^{-3}$
x	Number of cation atom	-
y	Number of anion atom	-
A^{y+}	Dissociate equivalent moles of cation	Mole
B^{x-}	Dissociate equivalent moles of cation	Mole
Λ	Molar conductivity	Siemens meter ² mole ⁻¹ ($S.m^2.mol^{-1}$)
Λ^0	Limiting molar conductivity	$S.m^2.mol^{-1}$
$\Lambda_{theo.}$	Theoretical molar conductivity	$S.m^2.mol^{-1}$
λ_+^0	Limiting molar conductivity of the cation	$S.m^2.mol^{-1}$
λ_-^0	Limiting molar conductivity of the anion	$S.m^2.mol^{-1}$
C_{actual}	Actual electrolyte concentration	Mole.meter ⁻³ ($mol.m^{-3}$)
ϵ_r	Relative permittivity	Unit less
ϵ_w	Relative permittivity of pure water	Unit less
ϵ_{sol}	Relative permittivity of the electrolyte solution	Unit less
ϵ_{cyto}	Relative permittivity of cell cytoplasm	Unit less
ϵ_{mem}	Relative permittivity of cell membrane	Unit less
ϵ_{wall}	Relative permittivity of cell wall	Unit less
δ	Phenomenological constant	Meter ³ .mole ⁻¹ ($m^3.mol^{-1}$)
f	Frequency	Hz
κ_{ideal}	DC Conductivity at infinite dilution	S/m
$\kappa_{expt.}$	Experimental DC Conductivity	S/m
S_s	Constant	Siemens mole ^{-0.5} meter ^{0.5} ($S.mol^{-0.5}.m^{0.5}$)
u	Dipole moment	Debye, D
ΔP_0	Turgor pressure	Atm
ΔP	Osmotic pressure difference between the cell and the medium	Atm
P_e	Peclet number	Dimensionless number
a_c	Bacterial cell radius	Micrometer (μm)

ρ	Density	Gram/centimeter ³ (g/cm ³)
t	Time	Second (s)
T	Temperature	Kelvin (K)
K_b	Boltzmann constant	m ² kg s ⁻² K ⁻¹
x	Distance travelled by ions	Milimeter (mm)
D_s	Diffusivity/Diffusion Coefficient	$\mu\text{m}^2/\text{s}$
A	Radius of bacterial cytoplasm	Micrometer (μm)
a_{cyto}/a	Thickness of the bacterial cell cytoplasm	μm
a_{mem}	Thickness of the bacterial cell membrane	μm
a_{wall}	Thickness of the bacterial cell wall	μm
σ_{sol}	Medium conductivity	S/m
σ_{cyto}	Cell cytoplasm conductivity	S/m
σ_{mem}	Cell membrane conductivity	S/m
σ_{wall}	Cell wall conductivity	S/m
F_1/F_2	Cut-off frequency	Hertz (Hz)
Σ	Standard deviation	-
C_{LOD}	Limit of detection of impedance sensor	Milimolar (mM)
$S_{\text{impedance}}$	Sensitivity of impedance sensor	Ohms/mM
λ	Debye length	Nanometers, nm
π	A dimensionless quantity written as pi with value equal to 3.14	-
I_s	Ionic Strength	Molar (M)
N_b	Total number of cells in 20 microliter volume	-
D_{PDMS}	Radius of the PDMS chamber	μm
A_{PDMS}	Total surface area of the PDMS chamber	μm^2
A_{FOV}	Area per field of view	μm^2
N_b	Total number of cells	-
N	Total number of cells captured on the entire electrode surface	-
N_c	Total number of cells captured per field of view on electrode surface	-
n_{FOV}	Total number of field of view	-
N	Number of doubling cycles of bacteria	-
K	Intercept of zone of inhibition and antibiotic disk concentration plot	mm ²
m	Slope of zone of inhibition and antibiotic disk concentration plot	mm ² /μg
V	Molar volume of the solute	cm ³ /gmol
J	Diffusion flux	Mol.m ⁻² .s ⁻¹
B_1 and B_0	Number of bacterial colonies formed at 160 and 0 min	-

ABBREVIATIONS

COVID-19 – Coronavirus disease 2019

WHO – World Health Organization

CDC – Centre for Disease Control and Prevention

AMR – Antimicrobial resistance

MS – Mass spectrophotometry

PCR – Polymerase chain reaction

ELISA – Enzyme-linked immunosorbent assay

FISH – Fluorescence in situ hybridization

AST– Antibiotic susceptibility testing

MIC – Minimum inhibitory concentration

CLSI – Clinical and Laboratory Standards Institute

R – Resistant strain/bacterium

S – Susceptible strain/bacterium

EUCAST – European Committee on AST

ZOI – Zone of inhibition

FDA – Food and Drug Administration

EF – Electric field

NPs – Nanoparticles

QCM – Quartz crystal microbalance

SPR – Surface plasmon resonance

POC – Point-of-care

PBS – Phosphate buffer saline

DI –Deionized

MBC – Minimum bactericidal concentration

LCGB – low conductivity growth buffer

LB – Lysogeny broth

DEP – Dielectrophoresis

HEPES – 4-(2-hydroxyethyl)-1-piperazineethanesulfonic acid

EPPS – 4-(2-hydroxyethyl)-1-piperazinepropanesulfonic acid

PIPES – 1,4-Piperazinediethanesulfonic acid

POPSO – Piperazine-1,4-bis (2-hydroxy-propanesulfonic acid) dihydrate

IDEs – Interdigitated electrodes

PDMS – Polydimethylsiloxane

DFT – Density functional theory

GGA – Hybrid generalized-gradient approximation

CM5 – Charge model 5

C-PCM – Conductor-like polarizable continuum model

MS – Mechanosensitive

DC – Direct current

AC – Alternative current

EDL – Electrical double layer

EP – Electrode polarization

DL – Double layer

CP – Counterion polarization

DLC – Double layer capacitance

MMT – Maxwell's mixture theory

ECM – Equivalent circuit modeling

FEM – Finite element method

ITO – Indium tin oxide

LOD – Limit of detection

AMPs – Antimicrobial peptides

Conc. – Concentration

nL – Nano-liters

pL – Pico-liters

mV – Millivolts

S/N – Signal to noise ratio

EC – *E. coli*

SA – *S. aureus*

KP – *K. pneumonia*

pDEP – Positive DEP

nDEP – Negative DEP

TSB – Tryptic soy broth

MHB – Mueller-Hinton broth

CM – Clausius–Mossotti factor

O.D. – Optical density

PMB – Polymyxin B sulfate

Sushi – Sushi S3 peptide

Bac – Bacitracin

Levo – Levofloxacin

MET – Methicillin

VA – Vancomycin

CMS – Colistin methanesulfonate

CF – Cefoxitin

AMP – Ampicillin

IMP – Imipenem

RIF – Rifampicin

GEN – Gentamicin

TR – Trimethoprim

CIP – Ciprofloxacin

MBC₁₀₀/BC₁₀₀ – Maximal bactericidal concentration

MBC₅₀/BC₅₀ – Half-maximal bactericidal concentration

MBC_{lysis}/BC_{lysis} – Lysis bactericidal concentration

DEPIS – Dielectrophoresis with impedance spectroscopy

LPS – Lipopolysaccharide molecules

OM – Outer membrane

FOV – Field of view

MSSA – Methicillin-susceptible *S. aureus*

MRSA – Methicillin-resistant *S. aureus*

EFS – Levo-susceptible *E. faecalis*

EFR – Levo-resistant *E. faecalis*

PBP – Penicillin-binding proteins

PI – Propidium iodide